

Full length article

Dissociated dislocation-mediated carbon transport and diffusion in austenitic iron

Ruiwen Xie^a, Song Lu^{*,a}, Wei Li^b, Yanzhong Tian^c, Levente Vitos^{a,b,d}^a Applied Materials Physics, Department of Materials Science and Engineering, Royal Institute of Technology, Stockholm SE-10044, Sweden^b Department of Physics and Astronomy, Division of Materials Theory, Uppsala University, Uppsala, Sweden^c Key Laboratory for Anisotropy and Texture of Materials (Ministry of Education), School of Materials Science and Engineering, Northeastern University, Shenyang 110819, China^d Wigner Research Centre for Physics, Institute for Solid State Physics and Optics, Budapest, Hungary

ARTICLE INFO

Article History:

Received 15 January 2020

Revised 5 March 2020

Accepted 24 March 2020

Available online 8 April 2020

Keywords:

Carbon-dislocation interaction

Stacking fault

Pipe diffusion

Twinning

ABSTRACT

Dislocation-solute interaction plays fundamental roles in mechanical properties of alloys. Here, we disclose the essential features of dislocation-carbon interaction in austenitic Fe at the atomistic scale. We show that passage of a Shockley partial dislocation in face-centered cubic iron is able to move carbon atoms on the slip plane forward by one Burgers vector, revealing a novel dissociated dislocation-mediated transport mechanism. This mechanism is induced by shear, which is distinct from the normal thermally activated diffusion process. Furthermore, we show that there exists a fast diffusion channel with significantly reduced diffusion energy barrier in the partial dislocation core, which is highly localized and directional. These inherent geometrical features are crucial for understanding the dependence of the diffusivity of dislocation pipe diffusion on the character of dislocations; most importantly, they can result in unbalanced pinning effect on the leading and trailing partials in a mixed dislocation, consequently facilitating stacking fault formation and deformation twinning. This explains the controversial effects of carbon on deformation twinning observed in various alloys. Our findings pave the road to tune mechanical properties of materials by manipulating dislocation-interstitial interaction.

© 2020 Acta Materialia Inc. Published by Elsevier Ltd. This is an open access article under the CC BY license. (<http://creativecommons.org/licenses/by/4.0/>)

1. Introduction

Carbon is undoubtedly one of the most important alloying elements in metallurgy, especially in steels. Thermodynamically, it is well accepted that C is a strong austenite stabilizer and noticeably increases the stacking fault energy (SFE) [1], consequently C addition should suppress deformation twinning (DT) in austenite according to the classical plasticity theory [2]. Controversially, it is often observed that C addition strongly promotes DT in various face-centered cubic (fcc) alloys including the important engineering alloys such as high-Mn twinning-induced plasticity (TWIP) steels [3–6], Fe–Ni–C austenitic steels [7] and the novel high/medium-entropy alloys like Fe–(30–40)Mn–10Co–10Cr (at.%) [8,9], CrMnFeCoNi [10,11] and CrCoNi [12]. The C-enhanced twinnability in these alloys is a crucial factor for the attainment of the high work-hardening capacity and the excellent mechanical properties such as a synergy of high strength and high ductility [5]. Although the exact microscopic mechanism remains elusive, the prominent effect of C on DT is usually

ascribed to dislocation-C interaction [5,6] which also underlies other fundamental strengthening mechanisms such as solid solution hardening [13], dislocation planar slip [2,14,15] and dynamic strain aging (DSA) [2,6]. Today, the microscopic features and mechanisms of dislocation-C interaction, especially at the dislocation core, are generally unclear and not accessible by experiments [16]. The lack of essential understanding of dislocation-C interaction has caused spirited disputes regarding the influence of C addition on the essential factors like the SFE, DT, DSA as well as martensitic phase transformation (MT) that strongly affect the plastic properties [2,5,6].

Dislocation is usually believed to significantly accelerate solute diffusion along the dislocation line, referred to as the dislocation pipe diffusion (DPD), which is ascribed to the reduced activation barrier [17–19]. The low activation barrier of DPD, normally assumed 40–80% of the corresponding bulk diffusion values for substitutional solutes and less than ~50% for interstitial elements [18–21], presumably originates from the distorted atomic structure or the presence of vacancies at the dislocation core [19]. However, recent studies elucidate that whether DPD can be faster than the normal bulk diffusion depends remarkably on the characteristics of the dislocation [22]. For example, screw dislocations in α -Fe were even shown

* Corresponding author.

E-mail address: songlu@kth.se (S. Lu).

to slow down hydrogen diffusion [23]. Similarly, atomistic simulations demonstrated that solute diffusion along the grain boundaries (GBs) can be either accelerated or inhibited, governed by the local GB structures at the atomic level [24].

In order to understand the influence of C on the aforementioned phenomena and processes, it is of significance to reveal the essential structural features that control C migration behavior at/near the dislocation core. In fcc materials with low SFEs, the $a/2 \langle 110 \rangle$ full dislocation normally dissociates into two $a/6 \langle 112 \rangle$ Shockley partials bounding a stacking fault (SF). Here, using quantum-mechanical ab initio calculations, we explore the migration behaviors of C in bulk, SF and partial dislocation core in the double-layer antiferromagnetic (AFMD) γ -Fe [25] with a focus of understanding the influence of C on dislocation mobility in high-Mn steels which have Néel temperatures at around room temperature [26,27]. We observe two striking consequences of the partial dislocation-C interaction, both of which arise from the fact that the Shockley partial dislocation exchanges the characteristics of the octahedral (O) and tetrahedral (T) interstitial sites after its passage. First, passage of a Shockley partial dislocation transfers the C atoms on the slip plane forward by a Burgers vector, which gives rise to a unprecedented dissociated dislocation-mediated mechanism for C transport. Second, the fast diffusion channel with significantly reduced energy barrier at the partial dislocation core is strongly localized and highly directional, i.e., perpendicular to the Burgers vector of the partial dislocation, which unveils the atomistic origin of the dependence of DPD on the characteristics of the dislocation. The above findings are crucial for understanding the observed C effects on dislocation planar slip, DSA, DT and MT in a consistent picture, which are beyond the thermodynamic role played by C.

2. Computational methodology

The equilibrium structure of AFMD γ -Fe with alternate two-layer collinear up- and down- spins along the [001] direction is fully relaxed. The obtained lattice and magnetic parameters are summarized in Appendix A Table A.1, in comparison with available data in literature. The AFMD γ -Fe is stabilized in the face-centered tetragonal structure, however, here it is still denoted as fcc for simplicity. The tetragonality is considered for all the calculations. The migration energy surface (MES) calculations are performed using a supercell with six (111) layers along the \mathbf{c} direction. The \mathbf{a} and \mathbf{b} lattice vectors of the supercell are $3 \times a/2[01\bar{1}]$ and $a[2\bar{1}1]$, respectively (Fig. 1 (A)). The generalized stacking fault (GSF) structures are created by tilting \mathbf{c} axis along the $[11\bar{2}]$ direction by the shear vector \mathbf{u} , i.e., $\mathbf{c} = \mathbf{c} + \mathbf{u}$ [28]. One C atom is placed on the slip plane. The nominal concentration of C is ~ 1.4 at% (~ 0.3 wt%), and the C–C interaction due to the periodic boundary conditions on the results is negligible. In order to obtain the MES, we calculate the total energy of the supercell by moving C step by step in the rectangular areas on the slip plane (Fig. 1 (A)). The MEP is then identified on the MES, which is a straight path along the $\langle 110 \rangle$ direction. This is consistent with the previous result obtained using the nudged elastic band method [29,30]. For the MES calculations, atomic relaxation to the second-nearest coordination shells of C is performed. With the current setup for modeling dislocation core/near-core structures, full atomic relaxation is not allowed. The effect of this constrained relaxation on the diffusion energy barriers is discussed in Appendix A, which does not affect our findings.

The AFMD configuration is known as the energetically most favorable collinear spin structure for γ -Fe, but in fcc Fe–Mn steels, it was demonstrated that with increasing Mn concentration the single-layer antiferromagnetic (AFMI) state becomes stable [27]. Additionally, the Néel temperature in high-Mn steels increases with Mn concentration [31]. In order to clarify the magnetic effect on the present problem, similar calculations have been performed for AFMI (Appendix B, Fig. B.1) and nonmagnetic (NM, Appendix B, Fig. B.2) structures. Magnetism is found to have a strong effect on the absolute values of bulk

diffusion barriers (see Appendix A, Table A.1), as well as C solution enthalpy [32] and SFE [33]. However, by comparing the calculated MES and MEP of AFMD γ -Fe with AFMI and NM γ -Fe, we see that magnetism has minor effect on our main findings. This observation is in line with experimental indications as well. For example, experimental studies for antiferromagnetic (AFM) and paramagnetic (PM) steels with different Mn concentrations at room temperature show that the magnetic state does not play a significant role on dislocation mobility. On the other hand, the dislocation mobility is strongly affected by C content [5,26]. Similar observation is made by changing temperature across the Néel temperature [34]. Further, the influence of C addition on twinning or DSA behavior in both AFM and PM steels are similar, indicating that the magnetic transition does not have a noticeable influence on the featured dislocation-C interaction in these alloys [5]. Furthermore, the MEP of C in ferromagnetic (FM) fcc Ni confirms the insignificant magnetic effect on our main conclusions (see Appendix B, Fig. B.3). Therefore, in the rest part of present work, we focus on results calculated at the AFMD state.

All the calculations are carried out using the Vienna ab-initio simulation package (VASP) [35,36]. The electron-ion interactions are described with the projector-augmented-wave method (PAW) [37,38]. The Perdew–Burke–Ernzerhof formula for the generalized gradient approximation is adopted for the exchange–correlation functional [39]. The energy cut-off for the plane-wave basis sets is 350 eV. The k-point mesh of $4 \times 4 \times 2$ for the supercell calculations is generated using the Monkhorst–Pack scheme [40]. The forces on atoms are converged to less than $0.02 \text{ eV } \text{\AA}^{-1}$ when atomic relaxation is allowed.

3. Results and discussion

3.1. Migration energy surface

When a leading partial dislocation with Burgers vector b_L glides towards a C atom on the close-packed $\{111\}$ plane, the local structural environment around the C atom evolves correspondingly. Specifically, the leading partial creates a SF after its passage. Here, we use the shear vector \mathbf{u} to measure the structure evolution from fcc ($\mathbf{u} = 0b_L$) to SF ($\mathbf{u} = 1b_L$) in a continuous way (Fig. 1). For $0b_L < \mathbf{u} < 1b_L$, it corresponds to the GSF, which models the partial dislocation core or near-core structures. It is important to observe that the leading partial transforms all the interstitial O sites on the slip plane in fcc lattice to the T sites in the SF (e.g., $1_{fcc}^O \rightarrow 1_{SF}^T$) and only half numbers of the neighboring T sites in fcc lattice to the O sites in the SF (e.g., $2_{fcc}^T \rightarrow 2_{SF}^O$), whereas the rest T sites maintain their character (e.g., $4_{fcc/SF}^T$, Fig. 1). Since C atoms prefer O sites in both fcc lattice and the SF [41], passage of a partial dislocation is expected to provoke the movement of the C atoms on the slip plane. The emerging question to address is when the process should happen, during or after the passage of the partial dislocation, which strongly affects how C atoms impede the mobility of both leading and trailing partials.

In order to probe the migration behavior of C as the local structure evolves from fcc to SF, we calculate the relevant MES (Fig. 2) in the rectangle areas 1K2I and 1K6J in Fig. 1 (A–C), with respect to \mathbf{u} . Here, \mathbf{u} is parallel to the $a/6[11\bar{2}]$ direction on the (111) slip plane, which has a significantly lower slip barrier than slipping along the $a/6[2\bar{1}1]$ direction due to the magnetic ordering in AFMD γ -Fe (Appendix A, Fig. A.1 (E)). For the same reason, the MES in the 1K2I and 1K6J areas are not symmetric (Fig. 2 (A–D)). In bulk ($\mathbf{u} = 0b_L$), the C atom occupies site 1^O as indicated by the energy minimum in Fig. 2 (A). The two neighboring T sites, 2_{fcc}^T and 6_{fcc}^T , are unstable for C. As the leading partial moving close to the C atom (increasing \mathbf{u}), the stable position for C gradually moves away from site 1 along the shear direction and changes to a position nearby site 2 (or 6) (Fig. 2 (B and C)). Notice that all the interstitial sites gradually lose the geometrical characters of O or T sites when \mathbf{u} approaches $0.5b_L$ (Fig. 2 (B)). For $\mathbf{u} = 1b_L$, interstitial sites 2 and 6 at the SF become the O sites, being the

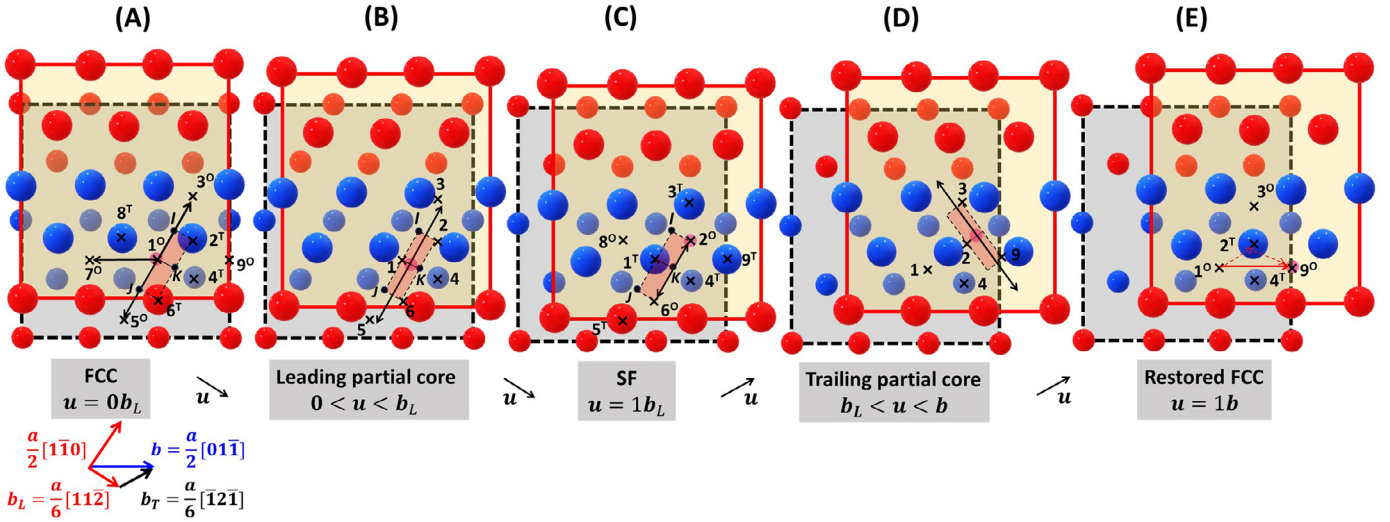


Fig. 1. Schematics of local atomic structure variation around a C atom during the passage of a pair of leading and trailing partial dislocations. The red and blue colors indicate the up- and down-spins, respectively, in the AFMD γ -Fe. The C atom is placed at the interstitial site between two (111) slip planes (small and large atoms, respectively). (A–E) The local structures for the original fcc ($u = 0b_L$, $b_L = a/6[112]$), leading partial core/near-core ($0 < u < b_L$), stacking fault ($u = 1b_L$), trailing partial core/near-core ($b_L < u < b$, $b = a/2[011]$) and restored fcc ($u = 1b$), respectively. Even and odd numbers denote the positions of the interstitial O and T sites, respectively, found on the slip plane in the fcc lattice. I and J denote the positions of crowdion sites on the $\langle 110 \rangle$ diffusion paths, $1_{fcc}^O \rightarrow 3_{fcc}^O$ and $1_{fcc}^O \rightarrow 5_{fcc}^O$, respectively, in the original fcc lattice. The migration energy surface (MES) is studied in the shaded rectangle areas (1K2I and 1K6J). (For interpretation of the references to color in this figure legend, the reader is referred to the web version of this article.)

energetically favorable positions for C (Fig. 2 (D)). It is important to observe that once u is larger than a critical value, $\sim 0.7b_L$ (Fig. 2 (C)), there is no energy barrier on the MES hindering the C atom moving from the vicinity of the original site 1 to the more stable positions near site 2 or 6, as the partial dislocation moves forward.

3.2. Dissociated dislocation-mediated transport of C

The above results clearly show that when a leading partial dislocation approaches a C atom on the slip plane, changing its surrounding environment from fcc to the GSF-like structures, the C atom will automatically adapt its position and shuffles from the original O site in fcc to the more stable position at the GSF. This movement of C is incorporated into the movement of the Fe atoms in the partial core upon external stress, therefore should occur instantly, that is, as fast as the speed of the dislocation. Notice that in the present magnetic configuration, a C atom has two potential final positions to choose, sites 2 and 6 (Fig. 2 (D)), which differ slightly in energy due to the local magnetic environment; and the final choice in metals and alloys should be affected by the fine dislocation core structures, local magnetic moments as well as chemistry [42]. Nevertheless, we can conclude that there is no thermodynamic or kinetic reason for C atoms to be transferred to (or left at) the unfavorable T sites (4_{SF}^T or 1_{SF}^T in Fig. 1 (C)) after the passage of a partial dislocation. Therefore, the present finding revokes all the previous arguments/mechanisms constructed on the assumption that the leading (/twinning) partials transfer C atoms to the unstable T sites in the SF (/twin) area [2,15,34,43]. For example, Adler et al. [43] ascribed the exceptionally large work hardening capacity in Hadfield steels to the tetragonal distortion caused by C atoms at the T sites in deformation twins. Lee et al. [15] argued that C atoms at the T sites at the SF area can easily hop to the O sites below the slip plane in Fe–Mn–C steels, which leads to the reorientation of Mn–C pairs and pinning of the trailing partial. Unfortunately, such unfounded microscopic picture has been widely adopted to explain the occurrence of DSA in high-Mn TWIP steels at room and lower temperatures when C bulk diffusion is too slow to account for the pinning process underlying DSA [2,6,15,34,44–46].

Following the same interaction mechanism between the leading partial and C atoms, when a trailing partial restores the local stacking

sequence from SF to fcc (Fig. 1 (C–E)), again it pushes C atoms in the SF area forward on the slip plane by one step, e.g., $2 \rightarrow 9$ in Fig. 1 (E). Therefore, the overall effect of passing a pair of partials is to displace the interstitial C atoms on the slip plane by a Burgers vector of $a/2 \langle 011 \rangle$, e.g., $1 \rightarrow 9$ in Fig. 1 (E), realizing the novel dissociated dislocation-mediated transport mechanism. In literature, it is generally accepted that at low strain rates, slowly moving dislocations can drag a cloud of solute atoms via bulk diffusion (Cottrell atmosphere) [13], whereas at high strain rates and low temperatures, the bulk diffusivity of solutes is too slow to catch up with the rapidly moving dislocations. Hence, the solutes are thought to be stationary [47]. Here, we reveal that in low-SFE materials, besides the thermally activated diffusion, moving dissociated dislocations provide an inherent shear-induced mechanism for the local transport of C atoms. This observation is in fact consistent with the nature of dislocations, that is to spatially transport mass as characterized by the Burgers vector. Considering the enormous numbers of dislocations during deformation, the currently disclosed mechanism can lead to significant redistribution of C atoms, especially at low temperatures when the thermally activated diffusion process is suppressed and dislocations are more prone to dissociate into partials. At high temperatures, more random jumps of C atoms will be stimulated, which can outweigh the dissociated dislocation-mediated C transport. Additionally, elevated temperature, thus higher SFE, promotes wavy slips of dislocations on different slip planes (more cross-slips), therefore less impact of the dissociated dislocation-mediate C transport is expected. By contrast, at low temperatures, smaller SFE promotes dislocation planar slip, thus contributing strongly to the C displacements on the slip plane. Furthermore, we envisage that successive passages of dissociated dislocations will gradually sweep C atoms away from dislocation sources like Frank-Read sources or GBs, which creates a C depletion area in the front of the source and generates a locally softened glide plane with low SFE and low frictional stress for subsequent dislocations. Consequently, the planarity of dislocation slip is amplified by the positive feedback due to this local C transport mechanism at the atomistic scale. The present finding offers a new perspective for understanding the effect of interstitials (C, N) on promoting planar slip in austenitic steels [48,49], which is distinct from the extant theories [2,50,51].

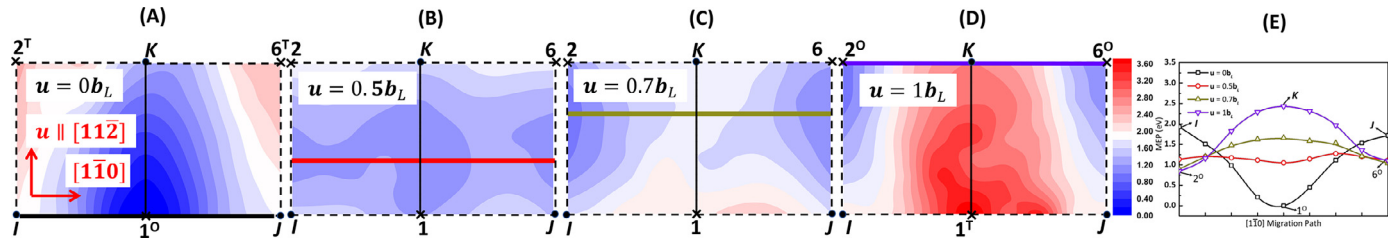


Fig. 2. Migration energy surface (MES) on the (111) slip plane. (A–D) The MES in the 1K2I and 1K6J rectangle areas in fcc ($u = 0b_L$), dislocation core/near-core ($u = 0.5b_L$ and $u = 0.7b_L$) and stacking fault ($u = 1b_L$), respectively. All the energies are relative to the total energy of the fcc structure with the C atom at the 1_{fcc} site. (E) The minimum migration energy path (MEP) for various u , as marked on the MES in (A–D) by the thick solid lines.

3.3. Fast diffusion channel

Previous studies showed that the MEP for C diffusion in bulk γ -Fe is a direct path along the $\langle 011 \rangle$ direction connecting two neighboring O sites with the transition state located at the crowding site [29,30], which is also confirmed in Fig. 2 (A). The obtained diffusion energy barriers along various $\langle 011 \rangle$ paths with different local magnetic configurations are consistent with the previous calculations [30] (for detailed comparison, see Appendix A, Table A.1). For $u > 0b_L$, the MEP is shifted along the slip direction, but maintains a nearly straight path (Fig. 2 (B–D)). Remarkably, in the representative partial core/near-core structures (Fig. 2 (B) and (C)), a fast diffusion channel with significantly reduced diffusion energy barriers is opened up. In particular, the diffusion energy barrier along the MEP for $u = 0.5b_L$ is ~ 0.22 eV, corresponding to $\sim 13\%$ of that for the same path in bulk (1.72 eV, Fig. 2 (E)). The formation of the fast diffusion channel mainly has a geometrical origin, which is verified by calculations at other magnetic states (see details in Appendices). An unstaggered avenue along the $\pm [110]$ directions is formed upon shearing along the Burgers vector of $a/6[11\bar{2}]$ at $u \approx 0.5b_L$, which locally removes the geometrical characteristics of the O and T sites and flattens the migration energy landscape. It provides a channel with large free volume which allows the interstitial C atoms to move easily [22]. The formation of such unstaggered avenue at the partial core was indeed observed in the previous molecular dynamics simulations [22,42,52]. We mention that in the real case, for example, when an edge partial dislocation generates asymmetrical compression and tension strain fields above and below the slip plane, one should not expect the perfect unstaggered channels in the core or near-core regions.

Importantly, the present work allows us to identify the critical geometrical features of the fast diffusion channel. From Fig. 2 (B and C), we observe that the fast diffusion channel at/near the partial dislocation core is highly directional, i.e., perpendicular to the Burgers vector of the partial dislocation. Inherently, the length of this channel is confined by the partial core width, $\sim |b_L|$ [24]; in other words, it is strongly localized in nature. Only when a partial is of pure edge character (90°), the localized diffusion channels are interconnected and form a long fast diffusion path along the dislocation line, otherwise, misalignment is expected between the localized fast diffusion channels and the dislocation line (Fig. 3 (A)). Consequently, the actual diffusivity of DPD along a single dislocation depends strongly on the dislocation character [20], and the net diffusion along a mixed dislocation line generally requires the aid of out-core diffusion [53,54], or of the local thermally activated vibrations of dislocation line itself [55]. We may mention that the present finding is akin to the recently disclosed roles of GBs in affecting hydrogen diffusion, showing that only high-angle GBs are able to facilitate hydrogen diffusion via forming interconnected low-barrier channels [24].

Interestingly, the SF ribbon itself also possesses lower in-plane diffusion barriers compared to those in bulk (Fig. 2 (E) and Appendix A, Table A.1), which is consistent with the previous theoretical and experimental results regarding the roles of SF in DPD in dissociated dislocations [19,53,56]. Considering that the outward-diffusion of C

atoms from the SF plane as driven by its effect on increasing the SFE is very slow at room temperature (“anti-suzuki effect” [57]), the fast redistribution of C at the SF is considered to be mostly confined between the two slip planes, similarly as self-interstitials and vacancies [19,20].

3.4. Unbalanced pinning

A significant consequence of presently disclosed geometric relationship between the fast diffusion channel and the Burgers vector of a partial dislocation is the unbalanced pinning effect (Fig. 3). In general, C impedes the movement of dislocations by introducing local lattice distortion and increasing the overall lattice frictional stress. When randomly distributed C atoms are incorporated into the dislocation core and redistribute to lower the total energy of the dislocation-C system, the dislocation is subject to an excess pinning force driven by magnetism or chemistry induced fluctuations on the migration energy surface along the dislocation line. The pinning force therefore depends on whether C atoms can effectively move to seek for the low-energy positions. When this process is sufficiently realized on the temporarily arrested dislocations, it can cause DSA [6,58,59]. We note that the bulk diffusivity of C in austenitic steels is extremely slow at room temperature due to the high activation barriers (see Appendix A, Table A.1), which can not account for the pronounced DSA effect as macroscopically manifested by the serrations on the stress-strain curves at room and cryogenic temperatures [6], whereas the redistribution within the localized fast diffusion channel can be easily accomplished as indicated by the very low migration energy barriers (Fig. 2 (E)). This excess pinning force is therefore maximized on the pure edge partial with fully interconnected fast diffusion channel along the dislocation line which efficiently facilitates C redistribution, while minimized on the pure

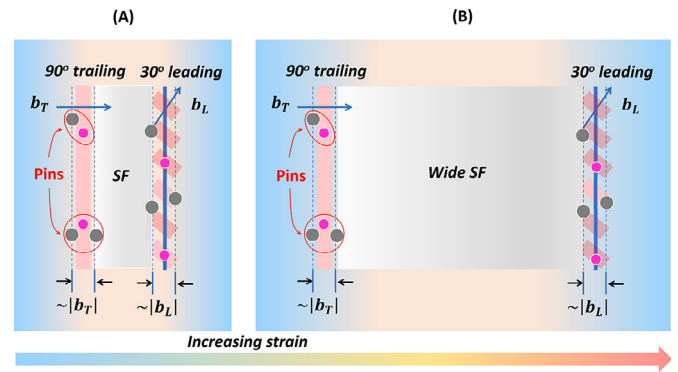


Fig. 3. Schematic for unbalanced pinning effect in a dissociated 60° dislocation. (A) The fully interconnected fast diffusion channel is formed along the 90° trailing partial line, which facilitates the formation of local pins including magnetic and chemical SROs via C fast redistribution in the core; whereas in the core of the 30° leading partial, the fast diffusion channels are not well connected to each other, thereby C diffusion is retarded and less pins can be formed. (B) A wide SF is formed between the two partials upon shearing, assisted by the unbalanced pinning effect.

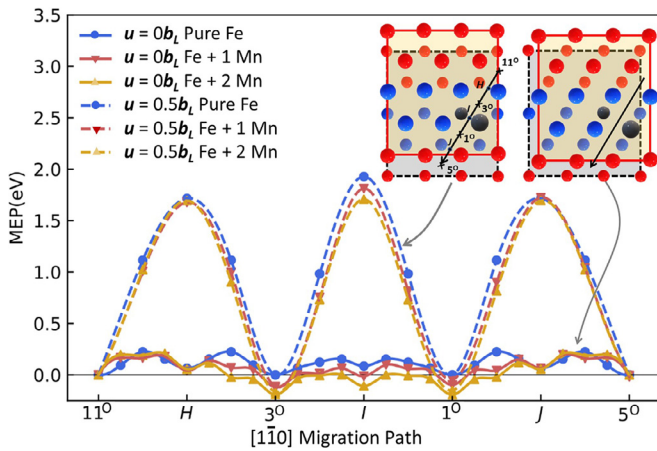


Fig. 4. Manganese-induced rugged migration energy landscape. Dashed and solid lines are the MEPs in bulk and partial core ($u = 0.5b_l$), respectively. Manganese atoms (gray balls) generate low energy sites and promotes C redistribution in the partial core, causing pinning.

screw partial with short and separated diffusion channels. As a consequence, the unbalanced (unequal) pinning is generally expected on the leading and trailing partials in a dissociated dislocation of mixed character (Fig. 3).

In AFMD γ -Fe, pure magnetism-induced energy variation between different potential (meta)stable positions for C in the core is small (~ 0.1 eV, Fig. 2 (E)). However, in alloys one can expect a remarkably uneven energy landscape with abundant attractive low-energy sites available in the core at finite temperatures, which is likely to be further enhanced when chemical and magnetic short range order (SRO) or fluctuations are met [60,61]. In Fig. 4, we demonstrate that even one or two Mn atoms can generate notably deeper pinning sites in the core, which will attract C atoms to form Mn-C SROs and obstruct the mobility of the partial. This is consistent with the previous ab initio studies showing that Mn and C atoms tend to form SROs in bulk γ -Fe [60]. Thereby, dislocations or segments with stronger pinning force on the trailing partials than that on the leading ones can be more easily separated into wide SF ribbons under applied stress, which consequently facilitates the nucleation of deformation twins or hexagonal close-packed (hcp, ϵ) martensites via the SF overlapping mechanisms (Fig. 3 (B)) [6,48,62]. Such unbalanced pinning-aided mechanism for DT is essential for understanding the observation that C addition notably promotes DT in various alloys, despite the fact that C increases the SFE [5–7,9–11,61]. The critical role of unbalanced pinning on DT is clearly demonstrated by the distinct deformation mechanisms in Fe-33Mn (wt.%, SFE = 37 mJ m⁻²) and Fe-33Mn-1.1C (wt.%, SFE = 57 mJ m⁻²) which are dislocation glide and DT, respectively [3]. Similar arguments apply for the deformation-induced γ - ϵ MT, where C was observed to accelerate the kinetics of the phase transformation [63,64]. In addition, we note that C addition causes solid solution hardening, increasing the flow stress, and thus the critical twinning stress may be reached at smaller strains in C-contained alloys. However, the solid solution hardening effect is usually weak for interstitial element in austenite [5]. Further, recent studies show that only ~ 0.2 – 0.8 at.% C addition can effectively promote DT [10–12], which obviously cannot be ascribed to the negligible solid solution hardening effect. We mention here that the unbalanced pinning effect should operate at relatively lower temperatures. At high temperatures, the diffusivity difference between pipe and bulk diffusion or between leading and trailing core is removed, thus the unbalanced pinning effect is not expected to be activated.

Since unbalanced pinning originates from C diffusion over the waiting time t_w when dislocations are temporarily arrested at obstacles, its strength should negatively depend on strain rate ($\dot{\epsilon}$). Here, t_w is inversely proportional to $\dot{\epsilon}$ [65]. Therefore, increasing strain

rate will suppress DT/MT via weakening the unbalanced pinning-aided mechanism, which is fully consistent with recent experimental observations in C-alloyed austenites [6,45,46,63,64]. For example, Yang et al. [45,46,66] showed that the density of twin boundary obviously decreases with increasing strain rate in Fe–Mn–C steels while little change or increase occurs in Fe–Mn–Al–Si or Fe–Mn–C–Al steels. Namely, in the alloys where no C exists or C diffusion is impeded by Al addition [67], the unbalanced pinning-aided twinning mechanism does not operate or is strongly suppressed. Given such circumstances, these alloys respond in a regular way as other fcc metals and interstitial-free alloys during deformation at various strain rates, i.e. DT is promoted by increasing strain rate [6,68]. A typical example is pure Al with very high SFE, in which DT rarely occurs even in nanoscales under normal deformation conditions, but macro-deformation twins can be activated under an ultrahigh strain rate [69]. Further, according to the dynamical Hall–Petch effect, the negative strain rate dependence of twin density in Fe–Mn–C alloys should lead to the negative strain rate sensitivity ($m = \partial \ln \sigma / \partial \ln \dot{\epsilon}$, where σ is the flow stress) [5,6], while in normal fcc metals and C-free Fe–Mn steels, the strain rate sensitivity is usually positive [45,46,66,68]. Similar arguments apply for MT in Fe–Mn–C transformation induced plasticity (TRIP) steels [64]. Such unusual strain rate dependence therefore provides a strong evidence of our proposed unbalanced pinning picture.

4. Conclusions

We studied the interaction mechanisms between partial dislocations and interstitial C atoms in γ -Fe and Fe–Mn steels at the atomistic scale. We discovered a so far unknown dissociated dislocation-mediated mechanism for C transport, which is crucial to account for the deformation-induced C redistribution, especially at low temperatures. This mechanism advances the current knowledge regarding the transport mechanism of interstitial elements, in addition to the normal diffusion process. Furthermore, we disclosed the fundamental features of the fast diffusion channel at the partial dislocation core. The highly localized and orientated nature of the fast diffusion channel results in the general unbalanced pinning effect on the dissociated dislocations in C-contained alloys, which assists SF and twinning formation and competes with the effect of C on increasing the SFE. This mechanism is not limited to γ -Fe or Fe–Mn steels, but can be generalized to other advanced alloys with excellent mechanical performance, such as the C-alloyed medium and high entropy alloys [8–12,61], for which the observations are also in perfect agreement with our theory. The present findings provide a physics-based understanding for the multiple roles played by C on DSA, dislocation planar slip and DT in various fcc alloys in a consistent picture and shed light on designing new alloys with interstitial-induced strengthening mechanisms.

Declaration of Competing Interest

The authors declare that they have no known competing financial interests or personal relationships that could have appeared to influence the work reported in this paper.

Acknowledgments

The authors thank Prof. Se Kyun Kwon and Prof. Han Soo Kim from POSTECH for valuable discussion. R.X. thanks Dr. Raquel Lizárraga for her advice on manuscript writing. S.L., R.X., W.L. and L.V. thank the Swedish Research Council, the Swedish Foundation for Strategic Research, the Carl Tryggers Foundations, the Swedish Foundation for International Cooperation in Research and Higher Education, the Hungarian Scientific Research Fund (OTKA 128229), and the China Scholarship Council for financial supports. S.L. and L.V. are

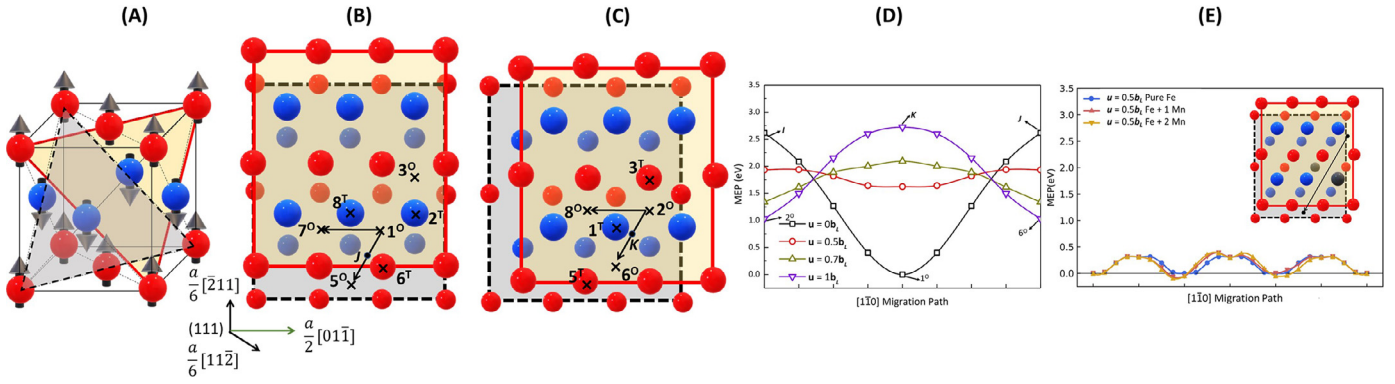


Fig. B.1. (A) Magnetic configuration of single-layer antiferromagnetic (AFMI) γ -Fe. (B) Two bulk diffusion paths for C exist due to the magnetic order. (C) Stacking fault via shearing by $a/6[112]$. Two different $\langle 110 \rangle$ diffusion paths are present in the SF plane. (D) MEP for various u in the range of $0-1b_L$, $b_L = a/6[112]$. (E) The effect of Mn alloying on the MEP in the dislocation core ($u = 0.5b_L$) in AFMI γ -Fe.

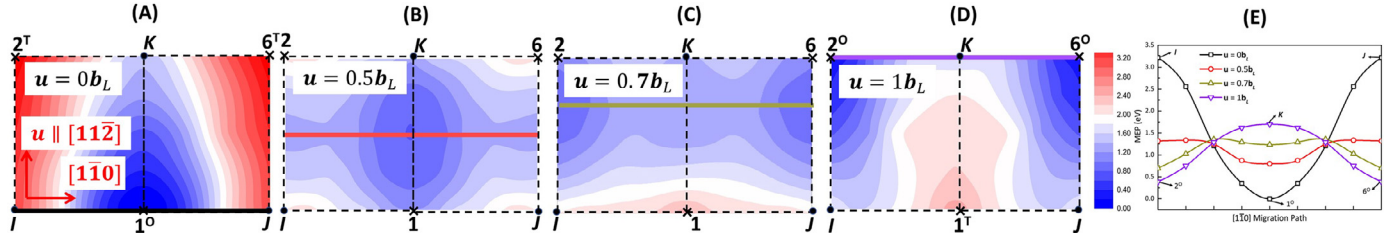


Fig. B.2. Migration energy surface in nonmagnetic γ -Fe. (A-D) The MES in the 1K2I and 1K6J rectangle areas in fcc ($u = 0b_L$), dislocation core/near-core ($u = 0.5b_L$ and $u = 0.7b_L$) and stacking fault ($u = 1b_L$), respectively, at the nonmagnetic (NM) state. 1K2I and 1K6J rectangle areas are symmetric. All the energies are relative to the total energy of the fcc structure with the C atom staying at the 1°_{fcc} site. (E) The MEP for various u , as indicated by the thick solid line on the MES in (A-D).

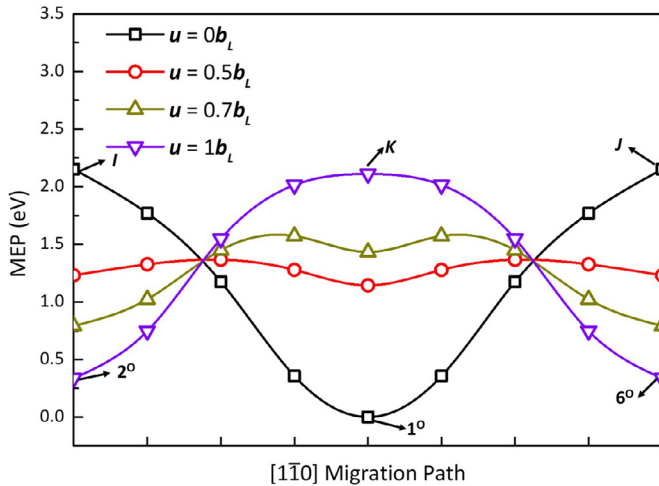


Fig. B.3. MEP for various u in ferromagnetic fcc Ni.

References

- [1] S. Lu, R. Li, K. Kdas, H. Zhang, Y. Tian, S.K. Kwon, K. Kokko, Q.-M. Hu, S. Hertzman, L. Vitos, Stacking fault energy of c-alloyed steels: the effect of magnetism, *Acta Mater.* 122 (2017) 72–81.
- [2] B.C.D. Cooman, Y. Estrin, S.K. Kim, Twinning-induced plasticity (TWIP) steels, *Acta Mater.* 142 (2018) 283–362.
- [3] M. Koyama, Y. Shimomura, A. Chiba, E. Akiyama, K. Tsuzaki, Room-temperature blue brittleness of Fe–Mn–C austenitic steels, *Scr. Mater.* 141 (2017) 20–23.
- [4] S.-J. Lee, J. Han, S. Lee, S.-H. Kang, S.-M. Lee, Y.K. Lee, Design for Fe-high Mn alloy with an improved combination of strength and ductility, *Sci. Rep.* 7 (2017) 3573.
- [5] O. Bouaziz, S. Allain, C. Scott, P. Cugy, D. Barbier, High manganese austenitic twinning induced plasticity steels: a review of the microstructure properties relationships, *Curr. Opin. Solid State Mater. Sci.* 15 (2011) 141–168.
- [6] M. Koyama, T. Sawaguchi, K. Tsuzaki, Overview of dynamic strain aging and associated phenomena in Fe–Mn–C austenitic steels, *ISIJ Int.* 58 (2018) 1383–1395.
- [7] A.K. Sachdev, M.M. Shea, Twinning in metastable Fe–Ni–C austenite during elevated temperature deformation, *Mater. Sci. Eng.* 95 (1987) 31–36.
- [8] Z. Li, C.C. Tasan, H. Springer, B. Gault, D. Raabe, Interstitial atoms enable joint twinning and transformation induced plasticity in strong and ductile high-entropy alloys, *Sci. Rep.* 7 (2017) 40704.
- [9] L. Chen, R. Wei, K. Tang, J. Zhang, F. Jiang, L. He, J. Sun, Heavy carbon alloyed fcc-structured high entropy alloy with excellent combination of strength and ductility, *Mater. Sci. Eng. A* 716 (2018) 150–156.
- [10] Z. Wu, C. Parish, H. Bei, Nano-twin mediated plasticity in carbon-containing FeNi–CoCrMn high entropy alloys, *J. Alloy. Compd.* 647 (2015) 815–822.
- [11] Z. Li, Interstitial equiatomic CoCrFeMnNi high-entropy alloys: carbon content, microstructure, and compositional homogeneity effects on deformation behavior, *Acta Mater.* 164 (2019) 400–412.
- [12] Y. Shang, Y. Wu, J. He, X. Zhu, S. Liu, H. Huang, K. An, Y. Chen, S. Jiang, H. Wang, X. Liu, Z. Lu, Solving the strength-ductility tradeoff in the medium-entropy NiCoCr alloy via interstitial strengthening of carbon, *Intermetallics* 106 (2019) 77–87.
- [13] A.H. Cottrell, B.A. Bilby, Dislocation theory of yielding and strain ageing of iron, *Proc. Phys. Soc. Sect. A* 62 (1949) 49.
- [14] S.I. Hong, C. Laird, Mechanisms of slip mode modification in fcc solid solutions, *Acta Metall. Mater.* 38 (1990) 1581–1594.
- [15] S.-J. Lee, J. Kim, S.N. Kane, B.C.D. Cooman, On the origin of dynamic strain aging in twinning-induced plasticity steels, *Acta Mater.* 59 (2011) 6809–6819.
- [16] D. Rodney, L. Ventelon, E. Clouet, L. Pizzagalli, F. Willaime, Ab initio modeling of dislocation core properties in metals and semiconductors, *Acta Mater.* 124 (2017) 633–659.
- [17] G. Love, Dislocation pipe diffusion, *Acta Metall.* 12 (1964) 731–737.
- [18] R.W. Balluffi, On measurements of self-diffusion rates along dislocations in fcc metals, *Phys. Status Solidi* 42 (1970) 11–34.
- [19] J. Huang, M. Meyer, V. Pontikis, Is pipe diffusion in metals vacancy controlled? A molecular dynamics study of an edge dislocation in copper, *Phys. Rev. Lett.* 63 (1989) 628–631.
- [20] R. Picu, D. Zhang, Atomistic study of pipe diffusion in Al–Mg alloys, *Acta Mater.* 52 (2004) 161–171.
- [21] M. Legros, G. Dehm, E. Arzt, T.J. Balk, Observation of giant diffusivity along dislocation cores, *Science* 319 (2008) 1646–1649.
- [22] A. Ishii, J. Li, S. Ogata, Conjugate channeling effect in dislocation core diffusion: carbon transport in dislocated BCC iron, *PLoS One* 8 (2013) e60586.
- [23] H. Kimizuka, S. Ogata, Slow diffusion of hydrogen at a screw dislocation core in α -iron, *Phys. Rev. B* 84 (2011) 024116.
- [24] X. Zhou, N. Mousseau, J. Song, Is hydrogen diffusion along grain boundaries fast or slow? atomistic origin and mechanistic modeling, *Phys. Rev. Lett.* 122 (2019) 215501.
- [25] D.W. Boukhvalov, Y.N. Gornostyrev, M.I. Katsnelson, A.I. Lichtenstein, Magnetism and local distortions near carbon impurity in γ -iron, *Phys. Rev. Lett.* 99 (2007) 247205.

- [26] S. Allain, O. Bouaziz, J. Chateau, Thermally activated dislocation dynamics in austenitic ferritic steels at low homologous temperature, *Scr. Mater.* 62 (2010) 500–503.
- [27] Y. Endoh, Y. Ishikawa, Antiferromagnetism of γ iron manganese alloys, *J. Phys. Soc. Jpn.* 30 (1971) 1614–1627.
- [28] S. Kibey, J. Liu, M. Curtis, D. Johnson, H. Sehitoglu, Effect of nitrogen on generalized stacking fault energy and stacking fault widths in high nitrogen steels, *Acta Mater.* 54 (2006) 2991–3001.
- [29] D.E. Jiang, E.A. Carter, Carbon dissolution and diffusion in ferrite and austenite from first principles, *Phys. Rev. B* 67 (2003) 214103.
- [30] D. Hepburn, D. Ferguson, S. Gardner, G. Ackland, First-principles study of helium, carbon, and nitrogen in austenite, dilute austenitic iron alloys, and nickel, *Phys. Rev. B* 88 (2013) 024115.
- [31] H. King, M. Peters, Predictive equations for martensitic and antiferromagnetic transformations in Fe–Mn–Al–Si alloys, *Can. Metall. Quart.* 36 (1997) 137–141.
- [32] A. Ponomareva, Y.N. Gornostyrev, I. Abrikosov, Ab initio calculation of the solution enthalpies of substitutional and interstitial impurities in paramagnetic fcc Fe, *Phys. Rev. B* 90 (1) (2014) 14439.
- [33] I. Bleskov, T. Hickel, J. Neugebauer, A. Ruban, Impact of local magnetism on stacking fault energies: a first-principles investigation for fcc iron, *Phys. Rev. B* 93 (2016) 214115.
- [34] I.-C. Jung, B.C.D. Cooman, Temperature dependence of the flow stress of Fe–18Mn–0.6C–xAl twinning-induced plasticity steel, *Acta Mater.* 61 (2013) 6724–6735.
- [35] G. Kresse, J. Hafner, Ab initio molecular dynamics for liquid metals, *Phys. Rev. B* 47 (1993) 558.
- [36] G. Kresse, J. Furthmüller, Efficient iterative schemes for *ab initio* total-energy calculations using a plane-wave basis set, *Phys. Rev. B* 54 (1996) 11169.
- [37] G. Kresse, D. Joubert, From ultrasoft pseudopotentials to the projector augmented-wave method, *Phys. Rev. B* 59 (1999) 1758.
- [38] P.E. Blöchl, Projector augmented-wave method, *Phys. Rev. B* 50 (1994) 17953.
- [39] J.P. Perdew, K. Burke, M. Ernzerhof, Generalized gradient approximation made simple, *Phys. Rev. Lett.* 77 (1996) 3865.
- [40] H.J. Monkhorst, J.D. Pack, Special points for Brillouin-zone integrations, *Phys. Rev. B* 13 (1976) 5188.
- [41] H. Gholizadeh, C. Draxl, P. Puschnig, The influence of interstitial carbon on the γ -surface in austenite, *Acta Mater.* 61 (2013) 341–349.
- [42] T. Smith, M. Hooshmand, B. Esser, F. Otto, D. McComb, E. George, M. Ghazisaeidi, M. Mills, Atomic-scale characterization and modeling of 60° dislocations in a high-entropy alloy, *Acta Mater.* 110 (2016) 352–363.
- [43] P.H. Adler, G.B. Olson, W.S. Owen, Strain hardening of hadfield manganese steel, *Metall. Mater. Trans. A* 17 (1986) 1725–1737.
- [44] J.-E. Jin, Y.K. Lee, Effects of Al on microstructure and tensile properties of C-bearing high Mn TWIP steel, *Acta Mater.* 60 (2012) 1680–1688.
- [45] H. Yang, Z. Zhang, Y. Tian, Z. Zhang, Negative to positive transition of strain rate sensitivity in Fe–22Mn–0.6C–x(Al) twinning-induced plasticity steels, *Mater. Sci. Eng. A* 690 (2017) 146–157.
- [46] H. Yang, Z. Zhang, F. Dong, Q. Duan, Z. Zhang, Strain rate effects on tensile deformation behaviors for Fe–22Mn–0.6C–(1.5Al) twinning-induced plasticity steel, *Mater. Sci. Eng.* 607 (2014) 551–558.
- [47] Y. Estrin, L. Kubin, Local strain hardening and nonuniformity of plastic deformation, *Acta Metall.* 34 (1986) 2455–2464.
- [48] I. Gutierrez-Urrutia, D. Raabe, Dislocation and twin substructure evolution during strain hardening of an Fe–22wt% Mn–0.6wt% C TWIP steel observed by electron channeling contrast imaging, *Acta Mater.* 59 (2011) 6449–6462.
- [49] U. Kocks, R. Cook, R. Mulford, Strain aging and strain hardening in Ni–C alloys, *Acta Metall.* 33 (1985) 623–638.
- [50] W. Owen, M. Grujicic, Strain aging of austenitic hadfield manganese steel, *Acta Mater.* 47 (1998) 111–126.
- [51] V. Gerold, H. Karnthaler, On the origin of planar slip in fcc alloys, *Acta Metall.* 37 (1989) 2177–2183.
- [52] H. Tsuzuki, P.S. Branicio, J.P. Rino, Molecular dynamics simulation of fast dislocations in copper, *Acta Mater.* 57 (2009) 1843–1855.
- [53] X. Zhang, G. Lu, Calculation of fast pipe diffusion along a dislocation stacking fault ribbon, *Phys. Rev. B* 82 (2010) 012101.
- [54] B.J. Heuser, D.R. Trinkle, N. Jalarvo, J. Serio, E.J. Schiavone, E. Mamontov, M. Tyagi, Direct measurement of hydrogen dislocation pipe diffusion in deformed polycrystalline Pd using quasielastic neutron scattering, *Phys. Rev. Lett.* 113 (2014) 25504.
- [55] K. Tapasa, Y. Osetsky, D. Bacon, Computer simulation of interaction of an edge dislocation with a carbon interstitial in α -iron and effects on glide, *Acta Mater.* 55 (2007) 93–104.
- [56] Y. Tang, J.A. El-Awady, Atomistic simulations of the interactions of hydrogen with dislocations in fcc metals, *Phys. Rev. B* 86 (2012) 174102.
- [57] T. Hickel, S. Sandlbes, R. Marceau, A. Dick, I. Bleskov, J. Neugebauer, D. Raabe, Impact of nanodiffusion on the stacking fault energy in high-strength steels, *Acta Mater.* 75 (2014) 147–155.
- [58] M. Koyama, T. Sawaguchi, K. Tsuzaki, Influence of dislocation separation on dynamic strain aging in a Fe–Mn–C austenitic steel, *Mater. Trans.* 53 (2012) 546–552.
- [59] Y.N. Dastur, W.C. Leslie, Mechanism of work hardening in hadfield manganese steel, *Metall. Trans. A* 12 (1981) 749–759.
- [60] J. von Appen, R. Dronskowski, Carbon-induced ordering in manganese-rich austenite – a density-functional total-energy and chemical-bonding study, *Steel Res. Int.* 82 (2011) 101–107.
- [61] Y. Ikeda, I. Tanaka, J. Neugebauer, F. Körmann, Impact of interstitial C on phase stability and stacking-fault energy of the CrMnFeCoNi high-entropy alloy, *Phys. Rev. Mater.* 3 (2019) 113603.
- [62] T. Byun, On the stress dependence of partial dislocation separation and deformation microstructure in austenitic stainless steels, *Acta Mater.* 51 (2003) 3063–3071.
- [63] J.-B. Seol, J. Jung, Y. Jang, C. Park, Influence of carbon content on the microstructure, martensitic transformation and mechanical properties in austenite/ ϵ -martensite dual-phase Fe–Mn–C steels, *Acta Mater.* 61 (2013) 558–578.
- [64] J. Seol, J. Kim, S. Na, C. Park, H. Kim, Deformation rate controls atomic-scale dynamic strain aging and phase transformation in high Mn TRIP steels, *Acta Mater.* 131 (2017) 187–196.
- [65] W.A. Curtin, D.L. Olmsted, L.G. Hector, A predictive mechanism for dynamic strain ageing in aluminium-magnesium alloys, *Nat. Mater.* 5 (2006) 875–880.
- [66] H. Yang, Y. Tian, Z. Zhang, Z. Zhang, Different strain rate sensitivities between Fe–22Mn–0.6C and Fe–30Mn–3Si–3Al twinning-induced plasticity steels, *Mater. Sci. Eng. A* 655 (2016) 251–255.
- [67] I. Jung, S.-J. Lee, B.C.D. Cooman, Influence of Al on internal friction spectrum of Fe–18Mn–0.6C twinning-induced plasticity steel, *Scr. Mater.* 66 (2012) 729–732.
- [68] S. Curtze, V.T. Kuokkala, Dependence of tensile deformation behavior of TWIP steels on stacking fault energy, temperature and strain rate, *Acta Mater.* 58 (2010) 5129–5141.
- [69] F. Zhao, L. Wang, D. Fan, B. Bie, X. Zhou, T. Suo, Y. Li, M. Chen, C. Liu, M. Qi, Macrodeformation twins in single-crystal aluminum, *Phys. Rev. Lett.* 116 (2016) 75501.
- [70] C. Wells, W. Batz, R.F. Mehl, Diffusion coefficient of carbon in austenite, *JOM* 2 (1950) 553–560.
- [71] J. Gren, A revised expression for the diffusivity of carbon in binary Fe–C austenite, *Scr. Metall.* 20 (1986) 1507–1510.
- [72] Y. Nakada, A. Keh, Serrated flow in Ni–C alloys, *Acta Metall.* 18 (1970) 437–443.
- [73] A.D. LeClaire, *Diffusion in Solid Metals and Alloys*, 26, Springer-Verlag, Berlin, 1990.